

# CacheFL: Efficient Federated Cache Model Fine-Tuning for Vision-Language Models

Mengjun Yi<sup>1</sup>, Hanwen Zhang<sup>1</sup>, Hui Dou<sup>2</sup>, Jian Zhao<sup>3</sup> and Furao Shen<sup>1</sup>

<sup>1</sup>School of Artificial Intelligence, Nanjing University, China

<sup>2</sup>Department of Computer Science and Technology, Nanjing University, China

<sup>3</sup>School of Electronic Science and Engineering, Nanjing University, China

{mengjunyi, hwzhang, huidou}@smail.nju.edu.cn, {jianzhao, frshen}@nju.edu.cn

## Abstract

Large pre-trained Vision-Language Models (VLMs), such as Contrastive Language-Image Pre-training (CLIP), have exhibited remarkable zero-shot performance across various image classification tasks. Fine-tuning these models on domain-specific datasets further enhances their effectiveness for downstream applications. However, fine-tuning in cloud environments raises significant concerns regarding data security and privacy. Federated Learning (FL) offers a decentralized solution by enabling model training across local clients without centralizing sensitive data, but the high communication and computation costs of transmitting full pre-trained models during training limit its scalability. Additionally, non-Independent and Identically Distributed (non-IID) data across local clients can negatively impact model convergence and performance. To address these challenges, we propose CacheFL, a novel federated learning method that replaces traditional full model fine-tuning with lightweight cache model fine-tuning. The cache model is initialized using a class-balanced dataset generated by a generative pre-trained model, effectively mitigating the impact of non-IID data. This cache model is then distributed to local clients for fine-tuning, and the updated parameters from each client are aggregated on the server and redistributed. With the updated cache model, the classification performance of CLIP is improved after just a few epochs. By limiting the training and communication to the cache model, CacheFL significantly reduces resource demands while ensuring data privacy and security. Extensive experiments conducted on ImageNet and 10 additional datasets demonstrate that CacheFL outperforms traditional approaches in terms of classification accuracy, resource efficiency, and privacy preservation.

## 1 Introduction

With the rapid advancement of artificial intelligence, Vision-Language Models (VLMs) [Zhang *et al.*, 2024] have emerged

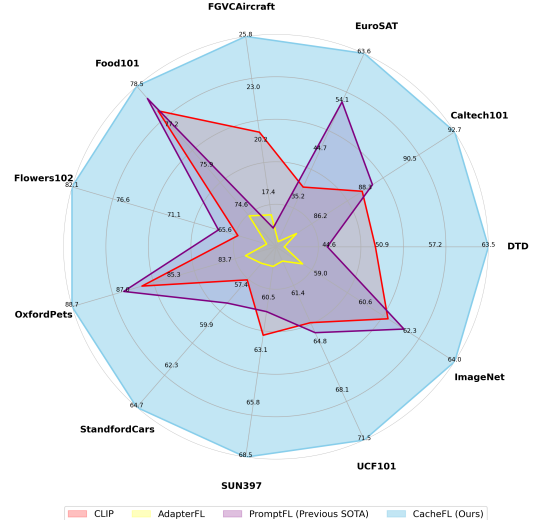


Figure 1: Performance comparison on the Extreme non-IID setting. Each axis denotes an accuracy value for the corresponding dataset (refer to Table 1). CacheFL surpasses state-of-the-art methods on 11 diverse image classification datasets.

as a key technology in multimodal learning, garnering significant attention in recent years. VLMs simultaneously model visual and linguistic signals, enabling cross-modal understanding between images and text. Among these, Contrastive Language-Image Pretraining (CLIP) [Radford *et al.*, 2021] has emerged as a representative and influential approach. By leveraging large-scale image-text pair datasets and employing contrastive learning techniques, CLIP demonstrates remarkable performance in tasks such as image classification. While CLIP exhibits strong generalization capabilities, its performance can often be further enhanced through fine-tuning on domain-specific datasets [Khattak *et al.*, 2023].

However, effective fine-tuning often requires access to diverse datasets distributed across various organizations or clients. Due to privacy, security, or storage constraints, these datasets are typically challenging to centralize in the cloud for training [Zhou *et al.*, 2019]. To overcome this limitation, Federated Learning (FL) [Kairouz *et al.*, 2021] has emerged as a promising paradigm for privacy-preserving and collab-

orative model optimization. FL enables multiple clients to train models locally on their private data and share updates to build a global model, ensuring that data remains “usable but invisible” during the distributed training process.

Despite its potential, directly applying FL to fine-tune CLIP and similar vision-language models presents two significant challenges. First, the large parameter sizes of these models create substantial communication and computation overheads in the federated learning framework [Chen *et al.*, 2021]. Second, the presence of non-Independent and Identically Distributed (non-IID) client data often results in slow convergence and limited performance gains in the global model [Li *et al.*, 2022].

To address these challenges, we propose **CacheFL**, a cache model-based federated learning fine-tuning method designed to optimize the fine-tuning process of CLIP and similar vision-language models in federated settings. This method first generates a class-balanced synthetic dataset using the generative pre-trained model [Ramesh *et al.*, 2021] on the server. Inspired by the TIP-Adapter method [Zhang *et al.*, 2021], we construct a lightweight cache model by the synthetic dataset on the server and distribute it to the clients. In contrast to fine-tuning the entire model, transmitting and training only the cache model significantly reduces both communication and computation overheads. Each client updates the cache model using its local data, and the parameter updates are subsequently aggregated on the server and redistributed to the clients. This iterative process enhances CLIP’s performance (Figure 1) while maintaining efficiency. The main works of this paper include the following:

- **We introduce a new cache model initialization approach.** This approach uses a generative pre-trained model to create a class-balanced synthetic dataset, enabling cache model initialization without the need for additional public or local datasets. It improves model robustness in non-IID scenarios, reduces data collection costs, and enhances data privacy protection.
- **We propose a novel federated learning fine-tuning method, CacheFL.** By replacing traditional full model fine-tuning with cache model fine-tuning, CacheFL significantly reduces communication and computation overhead while improving CLIP’s classification performance.
- **We conduct experiments on various image classification datasets under both IID and non-IID settings.** Experimental results demonstrate that our method excels in model performance, resource consumption, and data privacy protection, and effectively mitigates the challenges posed by data heterogeneity.

The remainder of this paper is organized as follows. Section 2 reviews related work on vision-language models and federated learning. Section 3 details the proposed method, and Section 4 presents experimental results that validate its effectiveness. Finally, Section 5 concludes the paper and discusses potential future research directions.

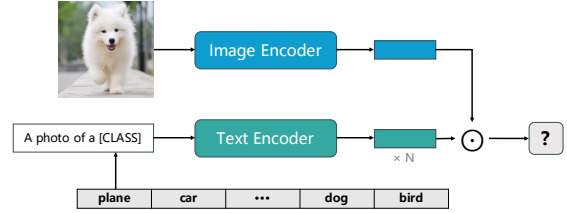


Figure 2: The Structure of CLIP. Each backbone contains an image encoder and a text encoder. Each encoder extracts feature representations from its respective modality. The model is trained to maximize the cosine similarity of the correct image-text pairs while minimizing the incorrect pairs.

## 2 Related Work

In this section, we review the foundational concepts, key methodologies, and relevant literature on vision-language models and federated learning.

### 2.1 Vision-Language Models

Vision-language models have demonstrated remarkable potential in the field of multimodal learning in recent years [Zhou *et al.*, 2022]. These models leverage joint learning of visual and linguistic features to tackle tasks such as image classification, image-text matching, and text generation.

A representative work in this domain is CLIP proposed by OpenAI [Radford *et al.*, 2021]. CLIP is a significant advance in multimodal machine learning that connects natural language and images. As shown in Figure 2, CLIP comprises two main components: Image Encoder and Text Encoder. The image encoder is often a convolutional neural network (CNN) or a vision transformer (ViT) [Dosovitskiy, 2020]. It takes an image input and maps it to a fixed-dimensional feature vector, or an embedding, in a latent space. The text encoder is typically a transformer-based architecture [Vaswani, 2017]. It takes a natural language input (a sentence or phrase) and similarly maps it to an embedding in the same latent space. The goal is for the corresponding image and text (e.g., a photo of a dog and the caption “a dog”) to have similar embeddings, while unrelated images and texts should be far apart in this space. CLIP is notable for its zero-shot prediction capabilities, meaning it can generalize to new tasks without explicit task-specific training. For classification, CLIP encodes an image into an embedding. Simultaneously, a set of possible class labels (e.g., “dog”, “cat”, “car”) is encoded by the text encoder into corresponding embeddings. The model then compares the similarity between the image embedding and each class embedding. The class with the highest similarity score is selected as the prediction.

While VLMs like CLIP excel in zero-shot learning scenarios, their performance can often be further enhanced through fine-tuning with task-specific data. Common fine-tuning methods can broadly be categorized into full fine-tuning and parameter-efficient fine-tuning [Ding *et al.*, 2023]. Full fine-tuning updates all model parameters to achieve optimal performance, but often requires substantial computational resources and may lead to overfitting, especially with limited data. In contrast, parameter-efficient fine-tuning adjusts

only a subset of the model’s parameters, thereby reducing resource consumption. Adapter tuning [He *et al.*, 2021] is a parameter-efficient fine-tuning method involving inserting additional small neural network modules, known as adapters, into the structure of a pre-trained model. During fine-tuning, only the parameters of these adapters are trained, while most of the pre-trained model’s parameters remain frozen. The CacheFL method proposed in this paper also belongs to an adapter tuning method. Additionally, prompt tuning [Lester *et al.*, 2021] is another method of parameter-efficient fine-tuning that guides the outputs of the pre-trained model by embedding task-specific prompt information into the input data. These prompts are either manually designed or trained using domain-specific datasets. However, regardless of the fine-tuning method employed, they often rely on downstream task data, which raises concerns about data security and privacy.

## 2.2 Federated Learning

Federated learning is a distributed machine learning framework that allows participants to collaboratively train models without sharing raw data, addressing privacy and security concerns in centralized learning [Li *et al.*, 2020a]. Data from different organizations, such as hospitals, cannot be centralized due to legal and regulatory constraints. Federated learning enables these entities to jointly train models while maintaining data privacy.

In federated learning, participants can process data and train models locally, transmitting only encrypted model parameters to a server for aggregation. The specific steps are as follows: first, the server initializes a global model and distributes it to participant devices. Subsequently, each device trains the model on its local data and updates its local model weights. Each device then sends its local model updates back to the server. The server receives updates from multiple devices and employs a specific aggregation algorithm to consolidate these updates into a new global model. This process is repeated until the model converges or meets predetermined performance criteria. Typically, the server uses the Federated Averaging algorithm (FedAvg) [McMahan *et al.*, 2017] to perform weighted average updates of the model parameters from each client. The FedAvg formula is as follows:

$$W^{t+1} = \sum_{k=1}^K \frac{n_k}{n} W_k^{t+1}, \quad (1)$$

where  $W^{t+1}$  represents the global model parameters at iteration  $t + 1$ ,  $K$  is the number of participating clients,  $n_k$  represents the number of samples on the  $k$ -th client,  $n$  represents the total number of samples on all clients and  $W_k^{t+1}$  denotes the local model parameters of the  $k$ -th client at iteration  $t + 1$ .

However, FL faces significant challenges when applied to resource-constrained clients, especially with large-scale models such as VLMs. These models often contain millions or even billions of parameters, leading to excessive communication and computation overhead during local training and model update transmission. To address these challenges, researchers have proposed integrating parameter-efficient fine-tuning techniques with FL. For instance, PromptFL [Guo *et*

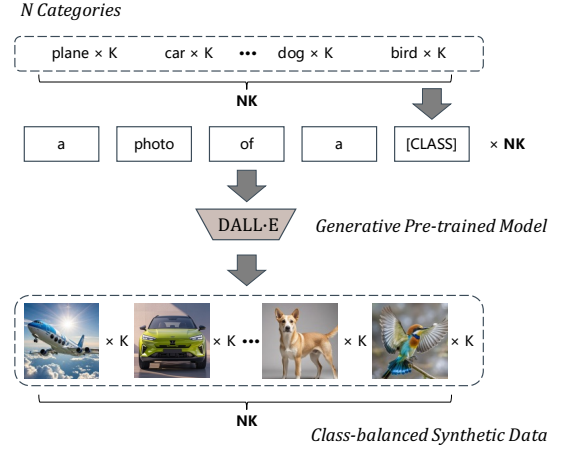


Figure 3: Class-balanced Synthetic Dataset Generation. We adopt DALL-E to generate  $K$  synthetic images for  $N$  categories separately.

*al.*, 2023] is a method that combines prompt tuning with federated learning, allowing multiple devices to fine-tune prompts instead of the CLIP model locally. Another significant challenge in FL is the non-IID data among the clients [Li *et al.*, 2022]. Heterogeneous data has a significant impact on the accuracy of FedAvg. Since the distribution of each local dataset may be different from the global distribution, the local objective of each client may be not consistent with the global optimal solution. As a result, there are drifts in the local updates. When local updates are large, the average model may be far from the global optimal solution. Li *et al.* [Li *et al.*, 2020b] proposed regularization techniques to mitigate data drift. However, these methods can only train from scratch without the pre-trained model and the final result is often limited. Thus, it is imperative to develop novel solutions that simultaneously address the dual challenges of resource constraints and non-IID data for the integration of FL with VLMs.

## 3 Methodology

In this section, we provide the details of our proposed method CacheFL and theoretically analyze the convergence of CacheFL.

### 3.1 Federated Cache Model Fine-Tuning

To further enhance the classification performance of CLIP and its similar structures, CacheFL introduces a three-step process: (1) A class-balanced synthetic dataset is generated on the server using a generative pre-trained model. (2) A lightweight cache model is built based on this synthetic dataset. (3) The cache model is distributed to clients, where local fine-tuning is performed on their private datasets. After local training, the updated model parameters are returned to the server and aggregated to optimize the global model. Detailed descriptions of each step are provided below.

**Class-Balanced Synthetic Dataset Generation.** Given the concerns regarding data security and privacy, the server often

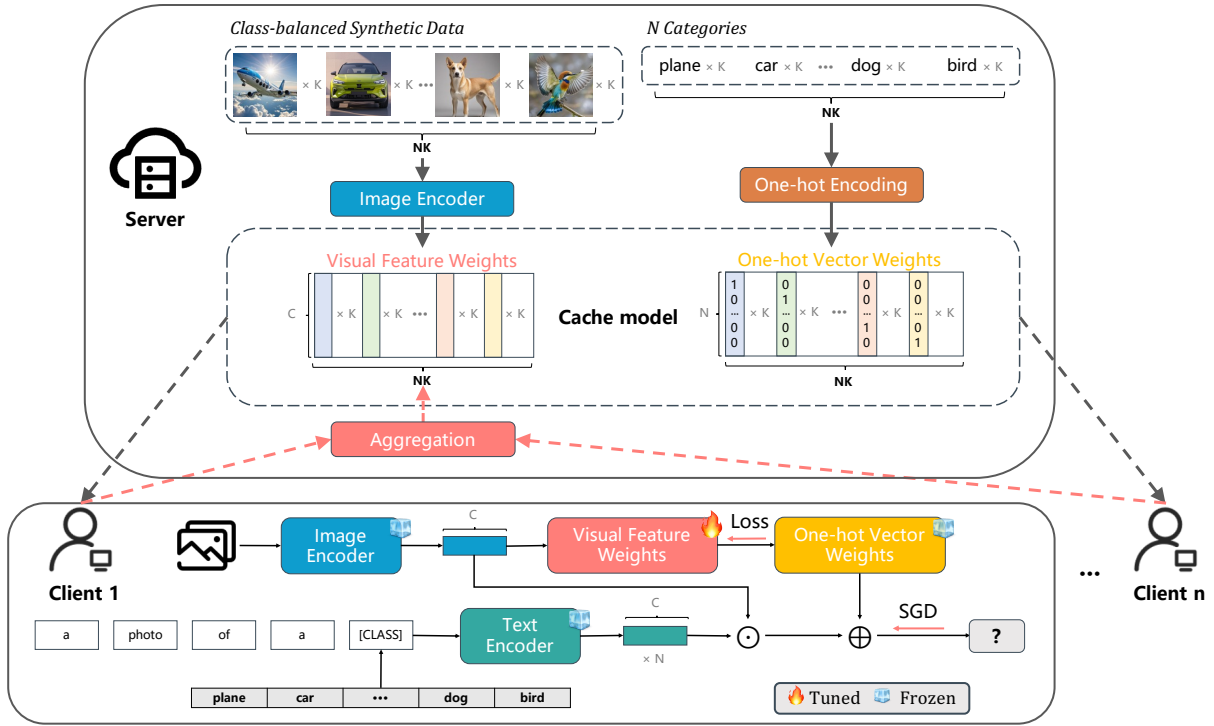


Figure 4: The workflow of CacheFL Federated Training. Each client includes a cache model (with the visual feature weights being trainable and the one-hot vector weights remaining frozen) and an out-of-the-box CLIP (with the backbone remaining frozen). The server aggregates the updates to the visual feature weights from multiple clients, and then transmits the updated parameters back to each client for further local processing.

lacks sufficient high-quality data for model training. Moreover, collecting public datasets is costly and may not ensure balanced class distributions. While Generative Adversarial Networks (GANs) [Goodfellow *et al.*, 2020] are widely used for data generation, their sample quality is often insufficient due to issues like mode collapse [Thanh-Tung and Tran, 2020], making them less practical for real-world use. In contrast, recent generative pre-trained models have shown greater potential in data generation, addressing challenges related to data scarcity and quality.

We employ the DALL·E generative pre-trained model from OpenAI for data generation. As illustrated in Figure 3, we input  $N$  class labels formatted as “a photo of a [CLASS]” into the DALL·E model, generating  $K$  images for each label, expressed as:

$$I_{N,K} = \text{DALL}\cdot E(T_N), \quad (2)$$

where  $T_N$  represents the textual input of the  $N$  class labels, and  $I_{N,K}$  represents the  $NK$  images generated for these labels. This method automatically creates a synthetic dataset with balanced class distributions, significantly reducing the manual data collection effort while ensuring diversity and balance in the dataset. This approach will mitigate potential bias caused by data scarcity or imbalance during federated learning, enhancing the generalization ability of the model.

**Cache Model Construction.** Directly fine-tuning all parameters of large pre-trained models like CLIP, though improving performance, demands enormous communication and computation resources. In contrast, adapter tuning provides a

more lightweight fine-tuning approach. Most of the original model’s parameters remain frozen, and only the adapter layers are trained, thus reducing overhead.

We use the class-balanced synthetic dataset to initialize a cache model, which serves as the adapter for CLIP. As shown in Figure 4, we extract visual features from the synthetic dataset of  $NK$  images using CLIP’s image encoder, where the feature dimension is  $C$ , expressed as:

$$W_1 = \text{ImageEncoder}(I_{N,K}), \quad (3)$$

where  $W_1$  is a matrix with  $C$  rows and  $NK$  columns, representing cached visual feature weights. Next, we convert the labels  $L_{N,K}$  of the  $NK$  images into one-hot encoded vectors, expressed as:

$$W_2 = \text{OneHot}(L_{N,K}), \quad (4)$$

where  $W_2$  is a matrix with  $N$  rows and  $NK$  columns, representing cached one-hot vector weights. The visual feature weights  $W_1$  and the one-hot vector weights  $W_2$  form a complete cache model. This cache model effectively stores prior knowledge in the class-balanced dataset, providing a robust foundation for subsequent federated fine-tuning.

**Federated Training.** While the cache model based on the synthetic dataset can enhance downstream task performance to some degree, the improvement is often limited. Leveraging real-world data distributed across clients can significantly boost the model’s performance.

To protect data privacy while using local data, we apply federated learning to optimize the cache model’s update pro-



Table 1: Performance of CacheFL Against Existing FL Method. We evaluate the performance in terms of accuracy on 11 datasets. We adopt three data partitioning methods, where “iid” stands for the IID setting, “dir” represents the Dirichlet non-IID settings, and “pat” denotes the Extreme non-IID setting. Absolute gains over PromptFL are indicated in **purple**.

(a) Average over 11 datasets				(b) ImageNet				(c) Caltech101				(d) DTD			
Method	iid	dir	pat	Method	iid	dir	pat	Method	iid	dir	pat	Method	iid	dir	pat
FedAvg	5.2	5.1	4.4	FedAvg	0.4	0.3	0.2	FedAvg	6.0	9.3	5.7	FedAvg	4.3	4.4	4.6
FedProx	10.3	9.8	7.3	FedProx	0.4	0.3	0.3	FedProx	19.4	15.8	20.0	FedProx	9.9	8.4	7.3
CLIP	60.8	60.8	60.8	CLIP	61.5	61.5	61.5	CLIP	88.2	88.2	88.2	CLIP	50.1	50.1	50.1
AdapterFL	56.1	56.2	56.2	AdapterFL	58.4	58.3	58.3	AdapterFL	85.6	85.0	85.0	AdapterFL	39.1	39.4	39.3
PromptFL	64.1	63.1	61.8	PromptFL	62.1	61.8	62.1	PromptFL	90.2	90.7	88.7	PromptFL	55.0	48.5	44.4
CacheFL	<b>73.6</b>	<b>70.9</b>	<b>69.4</b>	CacheFL	<b>64.3</b>	<b>64.0</b>	<b>64.0</b>	CacheFL	<b>92.8</b>	<b>92.6</b>	<b>92.7</b>	CacheFL	<b>66.0</b>	<b>65.2</b>	<b>63.5</b>
	<b>+9.5</b>	<b>+7.8</b>	<b>+7.6</b>		<b>+2.2</b>	<b>+2.2</b>	<b>+1.9</b>		<b>+2.6</b>	<b>+1.9</b>	<b>+4.0</b>		<b>+11.0</b>	<b>+16.7</b>	<b>+19.1</b>
(e) EuroSAT				(f) FGVCaircraft				(g) Food101				(h) Flowers102			
Method	iid	dir	pat	Method	iid	dir	pat	Method	iid	dir	pat	Method	iid	dir	pat
FedAvg	26.8	24.9	20.0	FedAvg	2.7	2.7	2.6	FedAvg	1.7	1.6	1.5	FedAvg	5.2	4.4	4.5
FedProx	42.8	49.3	21.2	FedProx	6.6	5.0	4.0	FedProx	1.6	1.8	1.7	FedProx	3.7	3.7	3.3
CLIP	37.4	37.4	37.4	CLIP	20.7	20.7	20.7	CLIP	77.7	77.7	77.7	CLIP	64.2	64.2	64.2
AdapterFL	25.9	26.2	26.7	AdapterFL	15.8	16.0	16.3	AdapterFL	74.5	74.3	74.3	AdapterFL	61.1	61.1	61.1
PromptFL	45.5	52.5	54.1	PromptFL	6.2	19.0	15.6	PromptFL	78.0	77.4	78.1	PromptFL	88.2	68.6	66.3
CacheFL	<b>81.6</b>	<b>66.2</b>	<b>63.6</b>	CacheFL	<b>29.3</b>	<b>26.6</b>	<b>25.8</b>	CacheFL	<b>78.5</b>	<b>78.5</b>	<b>78.5</b>	CacheFL	<b>94.2</b>	<b>90.9</b>	<b>82.1</b>
	<b>+36.1</b>	<b>+13.7</b>	<b>+9.5</b>		<b>+23.1</b>	<b>+7.6</b>	<b>+10.2</b>		<b>+0.5</b>	<b>+1.1</b>	<b>+0.4</b>		<b>+6.0</b>	<b>+22.3</b>	<b>+15.8</b>
(i) OxfordPets				(j) StanfordCars				(k) SUN397				(l) UCF101			
Method	iid	dir	pat	Method	iid	dir	pat	Method	iid	dir	pat	Method	iid	dir	pat
FedAvg	5.0	4.0	4.4	FedAvg	1.6	1.2	1.2	FedAvg	0.9	0.9	0.8	FedAvg	3.2	2.4	2.3
FedProx	8.9	5.1	8.2	FedProx	3.6	2.3	2.6	FedProx	0.9	0.8	0.8	FedProx	15.4	15.6	10.8
CLIP	86.4	86.4	86.4	CLIP	57.0	57.0	57.0	CLIP	62.3	62.3	62.3	CLIP	63.3	63.3	63.3
AdapterFL	83.1	83.1	83.0	AdapterFL	56.1	56.2	56.0	AdapterFL	59.1	59.2	58.8	AdapterFL	59.1	59.1	59.0
PromptFL	88.5	86.9	87.0	PromptFL	58.7	58.3	58.4	PromptFL	66.4	63.6	61.1	PromptFL	66.4	66.7	64.0
CacheFL	<b>89.5</b>	<b>88.3</b>	<b>88.7</b>	CacheFL	<b>66.0</b>	<b>64.5</b>	<b>64.7</b>	CacheFL	<b>70.1</b>	<b>69.1</b>	<b>68.5</b>	CacheFL	<b>77.6</b>	<b>74.2</b>	<b>71.5</b>
	<b>+1.0</b>	<b>+1.4</b>	<b>+1.7</b>		<b>+7.3</b>	<b>+6.2</b>	<b>+6.3</b>		<b>+3.7</b>	<b>+5.5</b>	<b>+7.4</b>		<b>+11.2</b>	<b>+7.5</b>	<b>+7.5</b>

cess. After initializing the cache model on the synthetic dataset, the server distributes it to each client. On the client side, images from local datasets are input into CLIP’s image encoder to generate  $C$ -dimensional image feature vectors  $f_{\text{vision}}$ . Simultaneously, the descriptive text “a photo of a [CLASS]” for  $N$  classes is input into CLIP’s text encoder to generate  $N$   $C$ -dimensional text feature vectors  $f_{\text{text}}$ , forming an  $N \times C$  matrix  $W_{\text{text}}$ . Next, the logits between the image feature vector and the class text feature vectors are computed as follows:

$$\text{logits}_1 = f_{\text{vision}} W_{\text{text}}^T. \quad (5)$$

Additionally, following the Tip-Adapter method [Zhang *et al.*, 2021], the logits for each image are computed using the cache model as:

$$\text{logits}_2 = \exp(-\beta(1 - f_{\text{vision}} W_1)) W_2^T, \quad (6)$$

where  $\beta$  is a modulating hyperparameter. This step is equivalent to calculating the Euclidean distance between the feature  $f_{\text{vision}}$  and the visual feature weights  $W_1$  from the synthetic dataset and then querying the corresponding value.

Finally, the logits from the pre-trained CLIP and the logits according to values retrieved from the cache model are fused to obtain the final prediction logits:

$$\text{logits} = \text{logits}_1 + \alpha \cdot \text{logits}_2, \quad (7)$$

where  $\alpha$  is a hyperparameter that can be adjusted depending on the task requirements. When there is a large discrepancy in style between the downstream task and the synthetic dataset,

a smaller  $\alpha$  is preferred, whereas a larger  $\alpha$  is suitable when the differences are smaller.

The cache model is optimized using cross-entropy loss  $\mathcal{L}(\cdot)$  and the Stochastic Gradient Descent (SGD) algorithm. During  $t$ -th round of local optimization, the one-hot vector weights  $W_2$  remain frozen, and only the visual feature weights  $W_1$  are updated on client  $k$  as follows:

$$W_{1,k}^{t+1} \leftarrow W_1^t - \eta \nabla \mathcal{L}(W_1^t; (\text{logits}, y)). \quad (8)$$

After completing the  $t$ -th round of local training, client  $k$  sends the updated parameters  $W_{1,k}^{t+1}$  back to the server for aggregation, similar to the formula 1 of FedAvg, as follows:

$$W_1^{t+1} \leftarrow \sum_{k \in S_t} \frac{n_k}{n} W_{1,k}^{t+1}. \quad (9)$$

### 3.2 The Convergence of CacheFL

Theorem 1 demonstrates the convergence of CacheFL, with a detailed definition and proof provided in the supplementary material. For simplicity, we use  $c$  to denote the parameters to be trained in the cache model, i.e., the visual feature weights  $W_1$ .

**Theorem 1.** Suppose Assumptions 1 to 4 hold. Choose  $\gamma = \max\{8\frac{L}{\mu} - 1\}$  and the learning rate  $\eta_t = \frac{2}{\mu} \frac{1}{t+\gamma}$ . Then the objective function of CacheFL satisfies

$$\mathbb{E}[F(\bar{c}_t)] - F^* \leq \frac{2L}{(t+\gamma)\mu} \left( \frac{B+C}{\mu} + 2L \|\bar{c}_1 - c^*\|^2 \right), \quad (10)$$

where

$$B = \sum_{k=1}^N p_k^2 \sigma^2 + 6L\Gamma + 8(E-1)^2 G^2, \quad (11)$$

$$C = \frac{N-K}{N-1} \frac{4}{K} E^2 G^2. \quad (12)$$

## 4 Experiments

In this section, we evaluate CacheFL on several public image classification datasets, comparing its performance with other methods. Additionally, we assess CacheFL’s resource consumption and privacy-preserving capabilities relative to alternative approaches. Furthermore, we examine the impact of using synthetic datasets and federated training on the overall effectiveness of the method.

### 4.1 Experimental Settings

**Datasets and Data Heterogeneity.** We conduct experiments for CacheFL on 11 widely used image classification datasets: ImageNet [Deng *et al.*, 2009], Caltech101 [Fei-Fei *et al.*, 2004], DTD [Cimpoi *et al.*, 2014], EuroSAT [Helber *et al.*, 2019], FGVCAircraft [Maji *et al.*, 2013], Food101 [Bossard *et al.*, 2014], Flowers102 [Nilsback and Zisserman, 2008], OxfordPets [Parkhi *et al.*, 2012], StanfordCars [Krause *et al.*, 2013], SUN397 [Xiao *et al.*, 2010], and UCF101 [Soomro, 2012]. To evaluate the robustness of our approach against data heterogeneity, we adopt three distinct methods of dataset partitioning:

- IID: Each client shares the same classes.
- Dirichlet non-IID: Data is partitioned randomly among clients using a Dirichlet distribution with  $Dir(0.1)$ .
- Extreme non-IID: Each client owns the independent and non-overlapping classes.

**Baselines and Implementation.** We perform a performance comparison between six approaches: FedAvg [McMahan *et al.*, 2017], FedProx [Li *et al.*, 2020b], CLIP [Radford *et al.*, 2021], AdapterFL (integrate adapter tuning with federated learning), PromptFL [Guo *et al.*, 2023], and CacheFL. In FedAvg and FedProx, we use ResNet-50 [He *et al.*, 2016] as the backbone for training from scratch. For methods based on CLIP, we adopt ResNet-50 as the image encoder and a transformer as the text encoder. All experiments are conducted using PyTorch on Tesla V100 SXM2 32GB GPU, with training performed using stochastic gradient descent (SGD) with a learning rate of 0.001. CacheFL adopts DALL·E to generate 16 synthetic images per category. For the two hyperparameters  $\alpha$  and  $\beta$ , we use the grid search to adjust the optimal values for each dataset.

**Evaluation Metrics.** We use accuracy as the primary metric to evaluate model performance. Resource consumption is assessed by communication cost and computation cost. To evaluate the security and privacy protection of CacheFL, we employ a representative gradient inversion attack [Zhu *et al.*, 2019] to attempt the reconstruction of raw training images, testing the model’s resilience to such attacks.

For a more detailed experimental setup refer to the supplementary material.

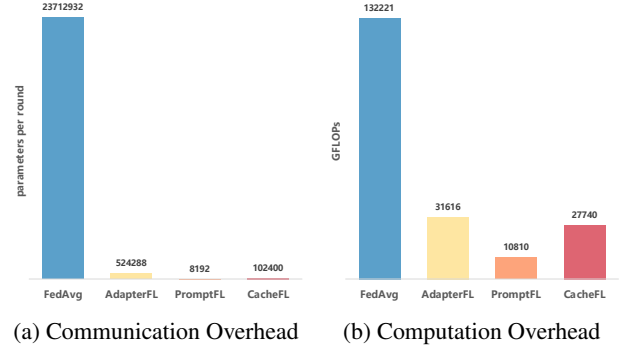


Figure 5: Resource Consumption. We evaluate the communication cost based on the number of parameters uploaded per round and the computation cost based on the Floating Point Operations (FLOPs) required for training.

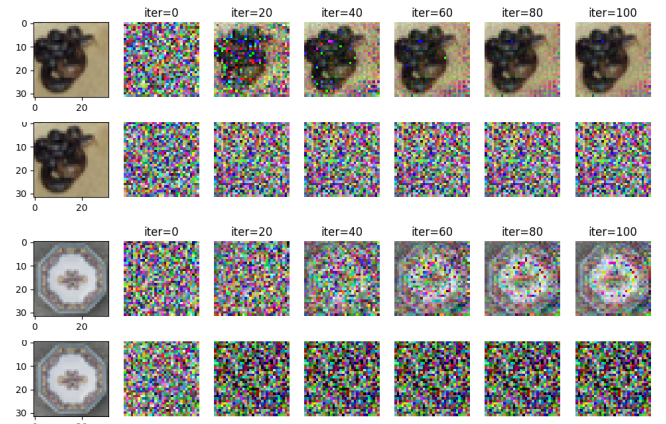


Figure 6: Gradient Inversion Attack. The top line of each image shows the results of FedAvg, where the attack almost recovers the raw image. The bottom line of each image presents the results of CacheFL, where the attack failed to reconstruct meaningful images.

### 4.2 Overall Performance

**Image Classification Performance.** Table 1 provides a comprehensive comparison of CacheFL against existing popular methods across multiple datasets under various data distributions. CacheFL consistently outperforms the baseline methods across all datasets and data distribution types. Moreover, CacheFL shows strong robustness to non-IID data distributions compared to PromptFL, which is evident in its performance on datasets such as DTD and Flowers102. In comparison, the performance of FedAvg and FedProx falls short across all datasets, primarily because these methods are not pre-trained and lack strong generalization capabilities. AdapterFL also demonstrates a decline in performance compared to the zero-shot CLIP model. This indicates that simply integrating adapter tuning with federated learning does not guarantee improvements on new tasks. In these scenarios, CacheFL surpasses its competitors, especially under more extreme data imbalances. These results highlight CacheFL’s good adaptability and generalization capabilities across diverse datasets.

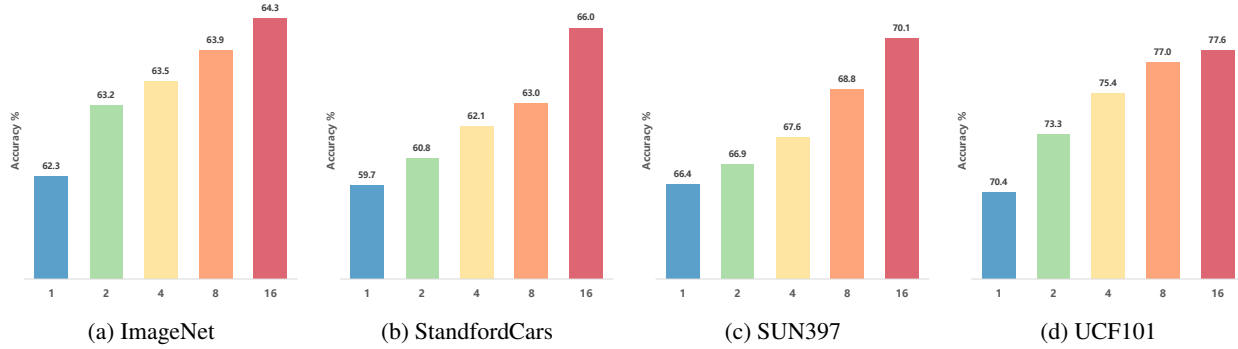


Figure 7: Performance with Synthetic Dataset. DALL-E generates images for each category in increments of 1 to 16.

**Communication and Computation Overhead.** Figure 5a illustrates the communication cost, quantified as the number of uploaded parameters per round, while Figure 5b depicts the computation cost, measured in Floating Point Operations (FLOPs) required for training. FedAvg imposes a significant communication burden of 23.7 million parameters per round and a training computation cost of 13,221 GB FLOPs, rendering it inefficient for large-scale federated learning applications. While PromptFL achieves the lowest communication and computation costs, it sacrifices some performance as seen in prior results. CacheFL, however, achieves an optimal balance between communication efficiency, computation efficiency, and model performance, demonstrating its scalability and practicality for federated learning in resource-constrained settings.

**Privacy Preservation.** We evaluate the privacy-preserving capabilities of CacheFL by applying a representative gradient inversion attack to reconstruct raw training images, following the method outlined by Zhu *et al.* [Zhu *et al.*, 2019]. To demonstrate the effect of defense, we compare the CacheFL approach with the FedAvg method. We utilize dummy data and labels and train for 100 iterations, recording reconstruction results at intervals of 20 epochs, as shown in Figure 6. The findings demonstrate that, with FedAvg, raw images can be almost recovered after a certain number of epochs, whereas the reconstructed images from CacheFL resemble noise. This indicates that CacheFL effectively preserves privacy through its cache model mechanism.

### 4.3 Ablation Study

**Performance with Synthetic Dataset.** Figure 7 presents the impact of the number of synthesized images generated by the DALL-E model on the accuracy of the CacheFL method on four datasets. As the number of synthesized images increases from 1 to 16 for each category, there is a clear upward trend in accuracy. The experimental results demonstrate that the more synthetic data samples we cache, the higher the accuracy CLIP with the cache model can achieve. However, the rate of improvement diminishes slightly beyond 8 images on the UCF101 datasets, indicating potential diminishing returns. This result suggests that while increasing the number of synthesized images can enhance performance, doing so indefinitely may not lead to continuous gains and could instead

result in higher computational costs. Therefore, identifying an optimal range for balancing performance improvements with computational efficiency is important.

**Performance with Federated Training.** Table 2 compares the performance of CacheFL with and without federated training across four datasets. CacheFL consistently outperforms the version without federated training on all datasets. Notably, the federated version achieves an accuracy of 77.6% on UCF 101, marking a substantial improvement of 19.7%. This significant improvement demonstrates the effectiveness of federated training in enhancing model generalization and performance by leveraging private data. The results suggest that federated training plays a critical role in maximizing the potential of CLIP.

Table 2: Performance with Federated Training. “w.o. Training” represents the method of not using federated training and only using the initial cache model.

	ImageNet	StanfordCars	SUN397	UCF101
<b>CacheFL</b>	<b>64.3</b>	<b>66.0</b>	<b>70.1</b>	<b>77.6</b>
w.o. Training	60.3	55.2	60.4	57.9

## 5 Conclusion

We propose CacheFL, a method for fine-tuning the CLIP model by integrating adapter tuning with federated learning. CacheFL preserves data privacy and security while effectively utilizing client knowledge to enhance the CLIP model’s performance on classification tasks. Furthermore, CacheFL addresses the issue of data heterogeneity in FL by employing class-balanced datasets generated by DALL-E and leveraging CLIP’s strong generalization capabilities. By transmitting only the cache model, rather than the full CLIP model, CacheFL significantly reduces communication and computation overhead during the FL process. In future work, we aim to improve the quality of the generated datasets, as their construction directly influences the cache model’s performance. For example, incorporating GPT [Achiam *et al.*, 2023] models to generate more diverse text descriptions could result in higher-quality images, further boosting CacheFL’s performance and applicability.

## Ethical Statement

There are no ethical issues.

## Acknowledgments

Omitted for anonymity.

## References

- [Achiam *et al.*, 2023] Josh Achiam, Steven Adler, Sandhini Agarwal, Lama Ahmad, Ilge Akkaya, Florencia Leoni Aleman, Diogo Almeida, Janko Altschmidt, Sam Altman, Shyamal Anadkat, et al. Gpt-4 technical report. *arXiv preprint arXiv:2303.08774*, 2023.
- [Bossard *et al.*, 2014] Lukas Bossard, Matthieu Guillaumin, and Luc Van Gool. Food-101—mining discriminative components with random forests. In *Computer vision—ECCV 2014: 13th European conference, zurich, Switzerland, September 6-12, 2014, proceedings, part VI 13*, pages 446–461. Springer, 2014.
- [Chen *et al.*, 2021] Mingzhe Chen, Nir Shlezinger, H Vincent Poor, Yonina C Eldar, and Shuguang Cui. Communication-efficient federated learning. *Proceedings of the National Academy of Sciences*, 118(17):e2024789118, 2021.
- [Cimpoi *et al.*, 2014] Mircea Cimpoi, Subhansu Maji, Iasonas Kokkinos, Sammy Mohamed, and Andrea Vedaldi. Describing textures in the wild. In *Proceedings of the IEEE conference on computer vision and pattern recognition*, pages 3606–3613, 2014.
- [Deng *et al.*, 2009] Jia Deng, Wei Dong, Richard Socher, Li-Jia Li, Kai Li, and Li Fei-Fei. Imagenet: A large-scale hierarchical image database. In *2009 IEEE conference on computer vision and pattern recognition*, pages 248–255. Ieee, 2009.
- [Ding *et al.*, 2023] Ning Ding, Yujia Qin, Guang Yang, Fuchao Wei, Zonghan Yang, Yusheng Su, Shengding Hu, Yulin Chen, Chi-Min Chan, Weize Chen, et al. Parameter-efficient fine-tuning of large-scale pre-trained language models. *Nature Machine Intelligence*, 5(3):220–235, 2023.
- [Dosovitskiy, 2020] Alexey Dosovitskiy. An image is worth 16x16 words: Transformers for image recognition at scale. *arXiv preprint arXiv:2010.11929*, 2020.
- [Fei-Fei *et al.*, 2004] Li Fei-Fei, Rob Fergus, and Pietro Perona. Learning generative visual models from few training examples: An incremental bayesian approach tested on 101 object categories. In *2004 conference on computer vision and pattern recognition workshop*, pages 178–178. IEEE, 2004.
- [Goodfellow *et al.*, 2020] Ian Goodfellow, Jean Pouget-Abadie, Mehdi Mirza, Bing Xu, David Warde-Farley, Sherjil Ozair, Aaron Courville, and Yoshua Bengio. Generative adversarial networks. *Communications of the ACM*, 63(11):139–144, 2020.
- [Guo *et al.*, 2023] Tao Guo, Song Guo, Junxiao Wang, Xueyang Tang, and Wenchao Xu. Promptfl: Let federated participants cooperatively learn prompts instead of models-federated learning in age of foundation model. *IEEE Transactions on Mobile Computing*, 2023.
- [He *et al.*, 2016] Kaiming He, Xiangyu Zhang, Shaoqing Ren, and Jian Sun. Deep residual learning for image recognition. In *Proceedings of the IEEE conference on computer vision and pattern recognition*, pages 770–778, 2016.
- [He *et al.*, 2021] Ruidan He, Linlin Liu, Hai Ye, Qingyu Tan, Bosheng Ding, Liying Cheng, Jia-Wei Low, Lidong Bing, and Luo Si. On the effectiveness of adapter-based tuning for pretrained language model adaptation. *arXiv preprint arXiv:2106.03164*, 2021.
- [Helber *et al.*, 2019] Patrick Helber, Benjamin Bischke, Andreas Dengel, and Damian Borth. Eurosat: A novel dataset and deep learning benchmark for land use and land cover classification. *IEEE Journal of Selected Topics in Applied Earth Observations and Remote Sensing*, 12(7):2217–2226, 2019.
- [Kairouz *et al.*, 2021] Peter Kairouz, H Brendan McMahan, Brendan Avent, Aurélien Bellet, Mehdi Bennis, Arjun Nitin Bhagoji, Kallista Bonawitz, Zachary Charles, Graham Cormode, Rachel Cummings, et al. Advances and open problems in federated learning. *Foundations and Trends® in Machine Learning*, 14(1–2):1–210, 2021.
- [Khattak *et al.*, 2023] Muhammad Uzair Khattak, Hanoona Rasheed, Muhammad Maaz, Salman Khan, and Fahad Shahbaz Khan. Maple: Multi-modal prompt learning. In *Proceedings of the IEEE/CVF Conference on Computer Vision and Pattern Recognition*, pages 19113–19122, 2023.
- [Krause *et al.*, 2013] Jonathan Krause, Michael Stark, Jia Deng, and Li Fei-Fei. 3d object representations for fine-grained categorization. In *Proceedings of the IEEE international conference on computer vision workshops*, pages 554–561, 2013.
- [Lester *et al.*, 2021] Brian Lester, Rami Al-Rfou, and Noah Constant. The power of scale for parameter-efficient prompt tuning. *arXiv preprint arXiv:2104.08691*, 2021.
- [Li *et al.*, 2020a] Li Li, Yuxi Fan, Mike Tse, and Kuo-Yi Lin. A review of applications in federated learning. *Computers & Industrial Engineering*, 149:106854, 2020.
- [Li *et al.*, 2020b] Tian Li, Anit Kumar Sahu, Manzil Zaheer, Maziar Sanjabi, Ameet Talwalkar, and Virginia Smith. Federated optimization in heterogeneous networks. *Proceedings of Machine learning and systems*, 2:429–450, 2020.
- [Li *et al.*, 2022] Qinbin Li, Yiqun Diao, Quan Chen, and Bingsheng He. Federated learning on non-iid data silos: An experimental study. In *2022 IEEE 38th international conference on data engineering (ICDE)*, pages 965–978. IEEE, 2022.
- [Maji *et al.*, 2013] Subhansu Maji, Esa Rahtu, Juho Kannala, Matthew Blaschko, and Andrea Vedaldi. Fine-



- grained visual classification of aircraft. *arXiv preprint arXiv:1306.5151*, 2013.
- [McMahan *et al.*, 2017] Brendan McMahan, Eider Moore, Daniel Ramage, Seth Hampson, and Blaise Agüera y Arcas. Communication-efficient learning of deep networks from decentralized data. In *Artificial intelligence and statistics*, pages 1273–1282. PMLR, 2017.
- [Nilsback and Zisserman, 2008] Maria-Elena Nilsback and Andrew Zisserman. Automated flower classification over a large number of classes. In *2008 Sixth Indian conference on computer vision, graphics & image processing*, pages 722–729. IEEE, 2008.
- [Parkhi *et al.*, 2012] Omkar M Parkhi, Andrea Vedaldi, Andrew Zisserman, and CV Jawahar. Cats and dogs. In *2012 IEEE conference on computer vision and pattern recognition*, pages 3498–3505. IEEE, 2012.
- [Radford *et al.*, 2021] Alec Radford, Jong Wook Kim, Chris Hallacy, Aditya Ramesh, Gabriel Goh, Sandhini Agarwal, Girish Sastry, Amanda Askell, Pamela Mishkin, Jack Clark, et al. Learning transferable visual models from natural language supervision. In *International conference on machine learning*, pages 8748–8763. PMLR, 2021.
- [Ramesh *et al.*, 2021] Aditya Ramesh, Mikhail Pavlov, Gabriel Goh, Scott Gray, Chelsea Voss, Alec Radford, Mark Chen, and Ilya Sutskever. Zero-shot text-to-image generation. In *International conference on machine learning*, pages 8821–8831. Pmlr, 2021.
- [Soomro, 2012] K Soomro. Ucf101: A dataset of 101 human actions classes from videos in the wild. *arXiv preprint arXiv:1212.0402*, 2012.
- [Thanh-Tung and Tran, 2020] Hoang Thanh-Tung and Truyen Tran. Catastrophic forgetting and mode collapse in gans. In *2020 international joint conference on neural networks (ijcnn)*, pages 1–10. IEEE, 2020.
- [Vaswani, 2017] A Vaswani. Attention is all you need. *Advances in Neural Information Processing Systems*, 2017.
- [Xiao *et al.*, 2010] Jianxiong Xiao, James Hays, Krista A Ehinger, Aude Oliva, and Antonio Torralba. Sun database: Large-scale scene recognition from abbey to zoo. In *2010 IEEE computer society conference on computer vision and pattern recognition*, pages 3485–3492. IEEE, 2010.
- [Zhang *et al.*, 2021] Renrui Zhang, Rongyao Fang, Wei Zhang, Peng Gao, Kunchang Li, Jifeng Dai, Yu Qiao, and Hongsheng Li. Tip-adapter: Training-free clip-adapter for better vision-language modeling. *arXiv preprint arXiv:2111.03930*, 2021.
- [Zhang *et al.*, 2024] Jingyi Zhang, Jiaying Huang, Sheng Jin, and Shijian Lu. Vision-language models for vision tasks: A survey. *IEEE Transactions on Pattern Analysis and Machine Intelligence*, 2024.
- [Zhou *et al.*, 2019] Zhi Zhou, Xu Chen, En Li, Liekang Zeng, Ke Luo, and Junshan Zhang. Edge intelligence: Paving the last mile of artificial intelligence with edge computing. *Proceedings of the IEEE*, 107(8):1738–1762, 2019.
- [Zhou *et al.*, 2022] Kaiyang Zhou, Jingkang Yang, Chen Change Loy, and Ziwei Liu. Learning to prompt for vision-language models. *International Journal of Computer Vision*, 130(9):2337–2348, 2022.
- [Zhu *et al.*, 2019] Ligeng Zhu, Zhijian Liu, and Song Han. Deep leakage from gradients. *Advances in neural information processing systems*, 32, 2019.

## A Theoretical Analysis

In this section, a detailed proof for Theorem 1 is provided.

### A.1 Definition

In this work, we consider the objective function of CacheFL:

$$\min_c \left\{ F(c) \doteq \sum_{k=1}^N p_k F_k(c) \right\}, \quad (13)$$

where  $N$  represents the number of clients and  $c$  represents the parameters of the cache model that need to be trained. The local objective  $F_k(\cdot)$  is defined by

$$F_k(c) \doteq \frac{1}{n_k} \sum_{j=1}^{n_k} \mathcal{L}(c; (x_{k,j}, y_{k,j})), \quad (14)$$

where the  $k$ -th device possesses  $n_k$  training data:  $(x_{k,1}, y_{k,1}), \dots, (x_{k,n_k}, y_{k,n_k})$ , and  $\mathcal{L}(\cdot)$  denotes the cross-entropy loss function.

In the context of a detailed federated learning process, during the  $t$ -th round, the procedure unfolds as follows: The server initially selects a subset of  $K$  clients at random, denoted as  $\mathcal{S}_t$ . Following this, the server broadcasts the parameters  $c_t$  to the participating clients. Each client  $k$  then initializes its local parameters as  $c_t^k = c_t$ . Thereafter, client  $k$  proceeds to conduct  $E$  rounds of local updates ( $i = 0, \dots, E-1$ ):

$$c_{t+i+1}^k \leftarrow c_{t+i}^k - \eta_{t+i} \nabla F_k(c_{t+i}^k, \xi_{t+i}^k), \quad (15)$$

where  $\eta_{t+i}$  is the learning rate and the  $\xi_{t+i}^k$  is sampled from the local dataset at client  $k$ . The server finally aggregates the received local cache models  $\{c_{t+E}^k | k \in \mathcal{S}_t\}$  and updates the global model  $\{c_{t+E}\}$  accordingly.

Let  $\mathcal{I}_E = \{nE | n = 1, 2, \dots\}$  be the set of synchronization rounds for the server-side, we can derive the update rule:

$$v_{t+1}^k = c_t^k - \eta_t \nabla F_k(c_t^k, \xi_t^k), \quad (16)$$

$$c_{t+1}^k = \begin{cases} v_{t+1}^k & \text{if } t+1 \notin \mathcal{I}_E, \\ \sum_{k \in \mathcal{S}_{t+1}} p_k \frac{N}{K} v_{t+1}^k & \text{if } t+1 \in \mathcal{I}_E. \end{cases} \quad (17)$$

The  $v_{t+1}^k$  represents the result of one step SGD, which is practically inaccessible. Also, we define  $\bar{g}_t = \sum_{k=1}^N p_k \nabla F_k(c_t^k)$  and  $g_t = \sum_{k=1}^N p_k \nabla F_k(c_t^k, \xi_t^k)$ . As a result,  $\bar{v}_{t+1} = \bar{c}_t - \eta_t g_t$  and  $\mathbb{E} g_t = \bar{g}_t$ .

### A.2 Assumption and lemmas

This section gives common assumptions used in federated learning as well as some necessary lemmas.

**Assumption 1.**  $F_i(i = 1, \dots, N)$  are all  $L$ -smooth, then, for all  $v$  and  $w$ ,  $F_i(v) \leq F_i(w) + (v - w)^\top \nabla F_i(w) + \frac{L}{2} \|v - w\|_2^2$ .

**Assumption 2.**  $F_i(i = 1, \dots, N)$  are all  $\mu$ -strongly convex, then, for all  $v$  and  $w$ ,  $F_i(v) \geq F_i(w) + (v - w)^\top \nabla F_i(w) + \frac{\mu}{2} \|v - w\|_2^2$ .

**Assumption 3.** The variance of local gradients is bounded:  $\mathbb{E} \|\nabla F_k(c_t^k, \xi_t^k) - \nabla F_k(c_t^k)\|^2 \leq \sigma_k^2$ .

**Assumption 4.** The expected squared norm of local gradients is bounded:  $\mathbb{E} \|\nabla F_k(c_t^k, \xi_t^k)\|^2 \leq G^2$ .

Assumption 1 and 2 represent canonical assumptions that are ubiquitously employed within the L2-normative paradigm of normalized linear regression coupled with softmax classification. Conversely, Assumption 3 and 4 are widely adopted in the context of federated learning frameworks.

**Lemma 1** (Results of one step SGD). *When Assumption 1 and 2 holds. If  $\eta_t \leq \frac{1}{4L}$ , we have*

$$\mathbb{E} \|\bar{v}_{t+1} - c^*\|^2 \leq (1 - \eta_t \mu) \mathbb{E} \|\bar{c}_t - c^*\|^2 + \eta_t^2 \mathbb{E} \|g_t - \bar{g}_t\|^2 + 6L\eta_t^2 \Gamma + 2\mathbb{E} \sum_{k=1}^N p_k \|\bar{c}_t - c_k^*\|^2 \quad (18)$$

where  $\Gamma = F^* - \sum_{k=1}^N p_k F_k^* \geq 0$ .

*Proof.* Considering that the  $\bar{v}_{t+1} = \bar{c}_t - \eta_t g_t$  holds,

$$\|\bar{v}_{t+1} - c^*\|^2 = \|\bar{c}_t - \eta_t g_t - c^* - \eta_t \bar{g}_t + \eta_t \bar{g}_t\|^2 \quad (19)$$

$$= \|\bar{c}_t - c^* - \eta_t \bar{g}_t\|^2 + \eta_t^2 \|g_t - \bar{g}_t\|^2 - 2\eta_t \langle \bar{c}_t - c^* - \eta_t \bar{g}_t, g_t - \bar{g}_t \rangle \quad (20)$$

According to  $\mathbb{E}g_t = \bar{g}_t$ ,  $\mathbb{E}[\langle \bar{c}_t - c^* - \eta_t \bar{g}_t, g_t - \bar{g}_t \rangle] = 0$ . On the other side,

$$\|\bar{c}_t - c^* - \eta_t \bar{g}_t\|^2 = \|\bar{c}_t - c^*\|^2 + \eta_t^2 \|\bar{g}_t\|^2 - 2\eta_t \langle \bar{c}_t - c^*, \bar{g}_t \rangle \quad (21)$$

From the Assumption 1, we have

$$\|\nabla F_k(c_t^k)\|^2 \leq 2L(F_k(c_t^k) - F_k^*) \quad (22)$$

The l2-norm is inherently a convex function, thus,

$$\eta_t^2 \|\bar{g}_t\|^2 \leq \eta_t^2 \sum_{k=1}^N p_k \|\nabla F_k(c_t^k)\|^2 \leq 2L\eta_t^2 \sum_{k=1}^N p_k (F_k(c_t^k) - F_k^*) \quad (23)$$

At the same time,

$$-2\eta_t \langle \bar{c}_t - c^*, \bar{g}_t \rangle = -2\eta_t \sum_{k=1}^N p_k \langle \bar{c}_t - c^*, \nabla F_k(c_t^k) \rangle \quad (24)$$

$$= -2\eta_t \sum_{k=1}^N p_k \langle \bar{c}_t - c_t^k, \nabla F_k(c_t^k) \rangle - 2\eta_t \sum_{k=1}^N p_k \langle c_t^k - c^*, \nabla F_k(c_t^k) \rangle \quad (25)$$

By Cauchy-Schwarz inequality and AM-GM inequality, we have

$$-2\langle \bar{c}_t - c_t^k, \nabla F_k(c_t^k) \rangle \leq \frac{1}{\eta_t} \|\bar{c}_t - c_t^k\|^2 + \eta_t \|\nabla F_k(c_t^k)\|^2 \quad (26)$$

From the Assumption 2, we have

$$-\langle c_t^k - c^*, \nabla F_k(c_t^k) \rangle \leq -(F_k(c_t^k) - F_k(c^*)) - \frac{\mu}{2} \|c_t^k - c^*\|^2 \quad (27)$$

Substitute the eqn.(26) and eqn.(27) into equation eqn.(25), and subsequently, introduce the results obtained, along with the eqn.(23), into eqn.(21), we have

$$\begin{aligned} \|\bar{c}_t - c^* - \eta_t \bar{g}_t\|^2 &\leq \|\bar{c}_t - c^*\|^2 + 2L\eta_t^2 \sum_{k=1}^N p_k (F_k(c_t^k) - F_k^*) \\ &\quad + \eta_t \sum_{k=1}^N p_k \left( \frac{1}{\eta_t} \|\bar{c}_t - c_t^k\|^2 + \eta_t \|\nabla F_k(c_t^k)\|^2 \right) \\ &\quad - 2\eta_t \sum_{k=1}^N p_k \left( F_k(c_t^k) - F_k(c^*) + \frac{\mu}{2} \|c_t^k - c^*\|^2 \right) \end{aligned} \quad (28)$$

$$\begin{aligned} &= (1 - \mu\eta_t) \|c_t^k - c^*\|^2 + \sum_{k=1}^N p_k \|\bar{c}_t - c_t^k\|^2 \\ &\quad + 4L\eta_t^2 \sum_{k=1}^N p_k (F_k(c_t^k) - F_k^*) - 2\eta_t \sum_{k=1}^N p_k (F_k(c_t^k) - F_k(c^*)) \end{aligned} \quad (29)$$

eqn.(28) to eqn.(29) are obtained from eqn.(22). Use the notation  $\Gamma = F^* - \sum_{k=1}^N p_k F_k^* \geq 0$ .

$$\begin{aligned} \|\bar{c}_t - c^* - \eta_t \bar{g}_t\|^2 &\leq (1 - \mu\eta_t) \|c_t^k - c^*\|^2 + \sum_{k=1}^N p_k \|\bar{c}_t - c_t^k\|^2 \\ &\quad - 2\eta_t (1 - 2L\eta_t) \sum_{k=1}^N p_k (F_k(c_t^k) - F_k^*) + 2\eta_t \sum_{k=1}^N p_k (F_k(c^*) - F_k^*) \end{aligned} \quad (30)$$

$$= (1 - \mu\eta_t) \|c_t^k - c^*\|^2 + \sum_{k=1}^N p_k \|\bar{c}_t - c_t^k\|^2 - 2\eta_t (1 - 2L\eta_t) \sum_{k=1}^N p_k (F_k(c_t^k) - F_k^*) + 4L\eta_t^2 \Gamma \quad (31)$$

Otherwise, the convexity of  $F_k(\cdot)$ , AM-GM inequality and eqn.(22) obtains

$$\sum_{k=1}^N p_k (F_k(c_t^k) - F^*) = \sum_{k=1}^N p_k (F_k(c_t^k) - F_k(\bar{c}_t)) + \sum_{k=1}^N p_k (F_k(\bar{c}_t) - F^*) \quad (32)$$

$$\geq \sum_{k=1}^N p_k \langle \nabla F_k(\bar{c}_t), \bar{c}_t^k - \bar{c}_t \rangle + F(\bar{c}_t) - F^* \quad (33)$$

$$\geq -\frac{1}{2} \sum_{k=1}^N p_k \left[ \eta_t \|\nabla F_k(\bar{c}_t)\|^2 + \frac{1}{\eta_t} \|\nabla c_t^k - \bar{c}_t\|^2 \right] + F(\bar{c}_t) - F^* \quad (34)$$

$$\geq -\sum_{k=1}^N p_k \left[ \eta_t L (F_k(\bar{c}_t) - F^*) + \frac{1}{2\eta_t} \|c_t^k - \bar{c}_t\|^2 \right] + F(\bar{c}_t) - F^* \quad (35)$$

Taking into account the following facts:  $\eta_t L - 1 \leq -\frac{3}{4} < 0$  and  $\sum_{k=1}^N p_k (F_k(\bar{c}_t) - F^*) = F(\bar{c}_t) - F^* \geq 0$ ,  $\Gamma \geq 0$  and  $4L\eta_t^2 + 2\eta_t(1 - 2L\eta_t)\eta_t L = 6L\eta_t^2 - 4L^2\eta_t^3 \leq 6L\eta_t^2$ , we have

$$\begin{aligned} & -2\eta_t(1 - 2L\eta_t) \sum_{k=1}^N p_k (F_k(c_t^k) - F^*) + 4L\eta_t^2 \Gamma \\ & \leq 2\eta_t(1 - 2L\eta_t) \sum_{k=1}^N p_k \left[ \eta_t L (F_k(\bar{c}_t) - F^*) + \frac{1}{2\eta_t} \|c_t^k - \bar{c}_t\|^2 \right] - 2\eta_t(1 - 2L\eta_t)(F(\bar{c}_t) - F^*) + 4L\eta_t^2 \Gamma \end{aligned} \quad (36)$$

$$= 2\eta_t(1 - 2L\eta_t)(\eta_t L - 1) \sum_{k=1}^N p_k (F_k(\bar{c}_t) - F^*) + (4L\eta_t^2 + 2\eta_t(1 - 2L\eta_t)\eta_t L)\Gamma + (1 - 2L\eta_t) \sum_{k=1}^N p_k \|c_t^k - \bar{c}_t\|^2 \quad (37)$$

$$\leq 6L\eta_t^2 \Gamma + \sum_{k=1}^N p_k \|c_t^k - \bar{c}_t\|^2 \quad (38)$$

Plugging eqn.(38) into eqn.(31), we have

$$\|\bar{c}_t - c^* - \eta_t \bar{g}_t\|^2 \leq (1 - \mu\eta_t) \|c_t^k - c^*\|^2 + 2 \sum_{k=1}^N p_k \|\bar{c}_t - c_t^k\|^2 + 6L\eta_t^2 \Gamma \quad (39)$$

Using eqn.(39) and taking expectation on both sides of eqn.(20), we have completed the proof of Lemma 1.  $\square$

**Lemma 2** (Bounding the variance). *When Assumption 3 holds. we have*

$$\mathbb{E} \|g_t - \bar{g}_t\|^2 \leq \sum_{k=1}^N p_k^2 \sigma^2. \quad (40)$$

*Proof.* Because the variance of local gradients is bounded, then

$$\mathbb{E} \|g_t - \bar{g}_t\|^2 = \mathbb{E} \left\| \sum_{k=1}^N p_k (\nabla F_k(c_t^k, \xi_t^k) - \nabla F_k(c_t^k)) \right\|^2 \quad (41)$$

$$= \sum_{k=1}^N p_k^2 \mathbb{E} \left\| \nabla F_k(c_t^k, \xi_t^k) - \nabla F_k(c_t^k) \right\|^2 \quad (42)$$

$$\leq \sum_{k=1}^N p_k^2 \sigma^2 \quad (43)$$

$\square$

**Lemma 3** (Bounding the divergence of  $\{c_t^k\}$ ). *When Assumption 4 holds. If  $\eta_t$  is non-increasing and  $\eta_t \leq 2\eta_{t+E}$  for all  $t \geq 0$ , we have*

$$\mathbb{E} \left[ \sum_{k=1}^N p_k \|\bar{c}_t - c_t^k\|^2 \right] \leq 4\eta_2(E-1)^2 G^2. \quad (44)$$

*Proof.* For any  $t \geq 0$ , there exists a  $t_0 \leq t$ , s.t.  $t - t_0 \leq E - 1$  and  $c_{t_0}^k = \bar{c}_{t_0}$  for all  $k = 1, 2, \dots, N$ .

$$\mathbb{E} \left[ \sum_{k=1}^N p_k \|\bar{c}_t - c_t^k\|^2 \right] = \mathbb{E} \left[ \sum_{k=1}^N p_k \|(c_t^k - \bar{c}_{t_0}) - (\bar{c}_t - \bar{c}_{t_0})\|^2 \right] \quad (45)$$

$$\leq \mathbb{E} \left[ \sum_{k=1}^N p_k \|c_t^k - \bar{c}_{t_0}\|^2 \right] \quad (46)$$

$$\leq \sum_{k=1}^N p_k \mathbb{E} \left[ \sum_{t=t_0}^{t-1} (E-1) \eta_t^2 \|\nabla F_k(c_t^k, \xi_t^k)\|^2 \right] \quad (47)$$

$$\leq \sum_{k=1}^N p_k \sum_{t=t_0}^{t-1} (E-1) \eta_{t_0}^2 G^2 \quad (48)$$

$$\leq \sum_{k=1}^N p_k \eta_{t_0}^2 (E-1)^2 G^2 \quad (49)$$

$$\leq 4\eta_t^2 (E-1)^2 G^2 \quad (50)$$

□

**Lemma 4** (Unbiased sampling scheme). *If  $t+1 \in \mathcal{I}_E$ , we have*

$$\mathbb{E}_{\mathcal{S}_t}(\bar{c}_{t+1}) = \bar{v}_{t+1}. \quad (51)$$

*Proof.* We sample  $x_k$  with probability  $q_k = \frac{1}{N}$  for each time. Let  $\mathcal{S}_t = \{i_1, \dots, i_K\} \subset [N]$ . Then

$$\mathbb{E}_{\mathcal{S}_t} \sum_{k \in \mathcal{S}_t} x_k = \mathbb{E}_{\mathcal{S}_t} \sum_{k=1}^K x_{i_k} = K \mathbb{E}_{\mathcal{S}_t} x_{i_1} = K \sum_{k=1}^N q_k x_k = \frac{K}{N} \sum_{k=1}^N x_k. \quad (52)$$

□

**Lemma 5** (Bounding the variance of  $\bar{c}_t$ ). *If  $\eta_t$  is non-increasing and  $\eta_t \leq 2\eta_{t+E}$  for all  $t \geq 0$ , the expected difference between  $\bar{v}_{t+1}$  and  $\bar{c}_{t+1}$  is bounded by*

$$\mathbb{E}_{\mathcal{S}_t} \|\bar{v}_{t+1} - \bar{c}_{t+1}\|^2 \leq \frac{N-K}{N-1} \frac{4}{K} \eta_t^2 E^2 G^2. \quad (53)$$

*Proof.* Suppose  $p_i = \frac{1}{N}, i = 1, 2, \dots, N$ , We have  $\bar{c}_{t+1} = \frac{1}{K} \sum_{k=1}^K v_{t+1}^{i_k}$ .

$$\mathbb{E}_{\mathcal{S}_t} \|\bar{v}_{t+1} - \bar{c}_{t+1}\|^2 = \mathbb{E}_{\mathcal{S}_t} \left\| \frac{1}{K} \sum_{i \in \mathcal{S}_{t+1}} v_{t+1}^i - \bar{v}_{t+1} \right\|^2 = \frac{1}{K^2} \mathbb{E}_{\mathcal{S}_t} \left\| \sum_{i=1}^N \mathbb{I}\{i \in \mathcal{S}_t\} (v_{t+1}^i - \bar{v}_{t+1}) \right\|^2 \quad (54)$$

$$= \frac{1}{K^2} \left[ \sum_{i \in [N]} \mathbb{P}(i \in \mathcal{S}_{t+1}) \|v_{t+1}^i - \bar{v}_{t+1}\|^2 + \sum_{i \neq j} \mathbb{P}(i, j \in \mathcal{S}_{t+1}) \langle v_{t+1}^i - \bar{v}_{t+1}, v_{t+1}^j - \bar{v}_{t+1} \rangle \right] \quad (55)$$

$$= \frac{1}{KN} \sum_{i=1}^N \|v_{t+1}^i - \bar{v}_{t+1}\|^2 + \sum_{i \neq j} \frac{K-1}{KN(N-1)} \langle v_{t+1}^i - \bar{v}_{t+1}, v_{t+1}^j - \bar{v}_{t+1} \rangle \quad (56)$$

$$= \frac{1}{K(N-1)} \left( 1 - \frac{K}{N} \right) \sum_{i=1}^N \|v_{t+1}^i - \bar{v}_{t+1}\|^2 \quad (57)$$

Which is using the following equalities:  $\mathbb{P}(i \in \mathcal{S}_{t+1}) = \frac{K}{N}$  and  $\mathbb{P}(i, j \in \mathcal{S}_{t+1}) = \frac{K(K-1)}{N(N-1)}$  for all  $i \neq j$ , and



$$\sum_{i \in [N]} \|v_{t+1}^i - \bar{v}_{t+1}\|^2 + \sum_{i \neq j} \langle v_{t+1}^i - \bar{v}_{t+1}, v_{t+1}^j - \bar{v}_{t+1} \rangle = 0.$$

$$\mathbb{E} \|\bar{v}_{t+1} - \bar{c}_{t+1}\|^2 = \frac{N}{K(N-1)} \left(1 - \frac{K}{N}\right) \mathbb{E} \left[ \frac{1}{N} \sum_{i=1}^N \|v_{t+1}^i - \bar{v}_{t+1}\|^2 \right] \quad (58)$$

$$\leq \frac{N}{K(N-1)} \left(1 - \frac{K}{N}\right) \mathbb{E} \left[ \frac{1}{N} \sum_{i=1}^N \|v_{t+1}^i - \bar{c}_{t_0}\|^2 \right] \quad (59)$$

$$\leq \frac{N}{K(N-1)} \left(1 - \frac{K}{N}\right) 4\eta_t^2 E^2 G^2 \quad (60)$$

□

### A.3 The proof of Theorem 1

*Proof.* Note that

$$\|\bar{c}_{t+1} - c^*\|^2 = \|\bar{c}_{t+1} - \bar{v}_{t+1} + \bar{v}_{t+1} - c^*\|^2 \quad (61)$$

$$= \|\bar{c}_{t+1} - \bar{v}_{t+1}\|^2 + \|\bar{v}_{t+1} - c^*\|^2 + 2\langle \bar{c}_{t+1} - \bar{v}_{t+1}, \bar{v}_{t+1} - c^* \rangle \quad (62)$$

Taking expectation over  $\mathcal{S}_{t+1}$ , the inner product is zero due to the unbiasedness of  $\bar{c}_{t+1}$ , which has been proved in Lemma 4.

If  $t+1 \notin \mathcal{I}_E$ ,  $A_1$  vanishes because of  $\bar{c}_{t+1} = \bar{v}_{t+1}$ . We use Lemma 1, Lemma 2, Lemma 3 to bound the second terms:

$$\mathbb{E} \|\bar{c}_{t+1} - c^*\|^2 = \mathbb{E} \|\bar{v}_{t+1} - c^*\|^2 \leq (1 - \eta_t \mu) \mathbb{E} \|\bar{c}_t - c^*\|^2 + \eta_t^2 B \quad (63)$$

where

$$B = \sum_{k=1}^N p_k^2 \sigma^2 + 6L\Gamma + 8(E-1)^2 G^2 \quad (64)$$

If  $t+1 \in \mathcal{I}_E$ , we additionally use Lemma 5 to bound the first terms:

$$\mathbb{E} \|\bar{c}_{t+1} - c^*\|^2 = \mathbb{E} \|\bar{c}_{t+1} - \bar{v}_{t+1}\|^2 + \mathbb{E} \|\bar{v}_{t+1} - c^*\|^2 \quad (65)$$

$$\leq (1 - \eta_t \mu) \mathbb{E} \|\bar{c}_t - c^*\|^2 + \eta_t^2 (B + C) \quad (66)$$

where

$$C = \frac{N-K}{N-1} \frac{4}{K} E^2 G^2 \quad (67)$$

Let  $\Delta_t = \mathbb{E} \|\bar{c}_t - c^*\|^2$ , we have

$$\Delta_{t+1} \leq (1 - \eta_t \mu) \Delta_t + \eta_t^2 (B + C) \quad (68)$$

For decreasing learning rates,  $\eta_t = \frac{\beta}{t+\gamma}$  for some  $\beta > \frac{1}{\mu}$  and  $\gamma > 0$  s.t.  $\eta_1 \leq \min\{\frac{1}{\mu}, \frac{1}{4L}\}$  and  $\eta_t \leq 2\eta_{t+E}$ . We're going to prove  $\Delta_t \leq \frac{v}{t+\gamma}$  where  $v = \max\{\frac{\beta^2(B+C)}{\beta\mu-1}, (\gamma+1)\Delta_1\}$ .

We use mathematical induction to prove that. When  $t = 1$ ,  $\Delta_1 \leq \max\{\frac{\beta^2(B+C)}{\beta\mu-1}, (\gamma+1)\Delta_1\}$  clearly holds. Assume that  $t$  holds for the inequality, we have

$$\Delta_{t+1} \leq (1 - \eta_t \mu) \Delta_t + \eta_t^2 (B + C) \quad (69)$$

$$= \left(1 - \frac{\beta\mu}{t+\gamma}\right) \frac{v}{t+\gamma} + \frac{\beta^2(B+C)}{(t+\gamma)^2} \quad (70)$$

$$= \frac{t+\gamma-\beta\mu}{(t+\gamma)^2} v + \frac{\beta^2(B+C)}{(t+\gamma)^2} \quad (71)$$

$$= \frac{t+\gamma-1}{(t+\gamma)^2} v + \left[ \frac{\beta^2(B+C)}{(t+\gamma)^2} - \frac{\beta\mu-1}{(t+\gamma)^2} v \right] \quad (72)$$

According to  $v \geq \frac{\beta^2(B+C)}{\beta\mu-1}$ , we have

$$\Delta_{t+1} \leq \frac{t+\gamma-1}{(t+\gamma)^2} v = \frac{(t+\gamma-1)(t+\gamma+1)}{(t+\gamma)^2(t+\gamma+1)} v = \frac{(t+\gamma)^2-1}{(t+\gamma)^2(t+\gamma+1)} v \quad (73)$$

$$\leq \frac{v}{t+\gamma+1} \leq \frac{v}{t+\gamma} \quad (74)$$

Then by the Assumption 1, we have

$$\mathbb{E}[F(\bar{c}_t)] - F^* \leq \frac{L}{2} \Delta_t \leq \frac{L}{2} \frac{v}{t + \gamma} \quad (75)$$

Specifically, if we choose  $\beta = \frac{2}{\mu}$ ,  $\gamma = \max\{8\frac{L}{\mu} - 1\}$ , then  $\eta_t = \frac{2}{\mu} \frac{1}{t + \gamma}$  and

$$\mathbb{E}[F(\bar{c}_t)] - F^* \leq \frac{2L}{(t + \gamma)\mu} \left( \frac{B + C}{\mu} + 2L \|\bar{c}_1 - c^*\|^2 \right). \quad (76)$$

□

## B Experimental Details

In this section, we provide a comprehensive introduction to the details of our experiment.

### B.1 The details of training data

The raw training data for all 11 datasets consists of 16 images per class.

- **IID**: The data is evenly distributed across all clients. Each client possesses an identical set of classes, with a relatively uniform distribution in quantity. For instance, in the case where 16 images are allocated to 10 clients, the first four clients are endowed with one image per class, whereas the subsequent six clients are provided with two images per class.
- **Dirichlet non-IID**: The data is partitioned randomly among clients using a Dirichlet distribution with  $Dir(0.1)$ .
- **Extreme non-IID**: Each client owns the non-overlapping classes. For instance, when distributing 100 classes across 10 clients, each client receives a distinct, non-overlapping set of 10 classes.

### B.2 The details of each method

The loss function is the cross-entropy loss, the optimizer is SGD and the local learning rate is 0.001.

- **FedAvg**: A widely used federated learning (FL) framework. ResNet-50 is employed as the backbone model, trained from scratch for 500 rounds, with each round consisting of one epoch.
- **FedProx**: An enhanced optimization method based on FedAvg, which introduces a proximal term to address challenges posed by non-IID data distributions. All other settings are the same as FedAvg, with the proximal term parameter  $\mu = 0.1$ .
- **CLIP**: The original CLIP model without any fine-tuning.
- **AdapterFL**: An adapter-based FL method for CLIP fine-tuning, which learns an adapter across clients. The adapter consists of two fully connected layers and two ReLU layers, integrated into the image encoder. The original CLIP model weights remain frozen, and only the adapter layers are updated during training. The global training includes 20 rounds, with one local epoch per round.
- **PromptFL**: A prompt-based FL method for CLIP fine-tuning, which learns a prompt across clients. The prompt consists of  $p$  learnable  $d$ -dimensional vectors, where  $d$  corresponds to the dimension of word embeddings in the text encoder (default is 512), and  $p$  is a hyperparameter (default is 16). Similar to AdapterFL, the global training consists of 20 rounds, with one local epoch per round.
- **CacheFL**: This method adopts DALL-E to generate 16 synthetic images for each category in the dataset. The cache model is initialized, and training follows Algorithm 1 with  $T = 20$  (global rounds) and  $E = 1$  (local epochs). Each dataset uses distinct values of  $\alpha$  and  $\beta$ . Here, examples are provided for a subset of the datasets: Caltech101:  $\alpha = 3, \beta = 1$ , DTD:  $\alpha = 2, \beta = 1$ , Imagenet:  $\alpha = 0.6, \beta = 1$ .

---

#### Algorithm 1 CacheFL

---

```
1: SERVER:
2: Server initializes the cache model  $W_1, W_2$  by the synthetic dataset
3: Server broadcasts the cache model  $W_1, W_2$  to all clients
4: for each communication round  $t = 1, 2, \dots, T$  do
5:    $\mathcal{S}_t \leftarrow$  Server selects a random subset of  $K$  clients
6:   Server broadcasts  $W_1^t$  to all selected clients
7:   for each client  $k \in \mathcal{S}_t$  parallelly do
8:      $W_{1,k}^{t+1} \leftarrow ClientUpdate(k, W_1^t)$ 
9:   end for
10:   $W_1^{t+1} \leftarrow \sum_{k \in \mathcal{S}_t} \frac{n_k}{n} W_{1,k}^{t+1}$ 
11: end for
12:
13: CLIENT:  $ClientUpdate(k, W_1^t)$ 
14: for each local epoch  $e = 1, 2, \dots, E$  on local data  $D_k$  do
15:    $f_{\text{vision}} = ImageEncoder(D_k)$   $\triangleright$  Obtain visual features
16:    $W_{\text{text}} = TextEncoder(Input_N)$   $\triangleright$  Obtain textual features
17:    $logits = f_{\text{vision}} W_{\text{text}}^T + \alpha \exp(-\beta(1 - f_{\text{vision}} W_1)) W_2^T$   $\triangleright$  Obtain the predicted logits
18:    $W_{1,k}^{t+1} \leftarrow W_1^t - \eta \nabla \mathcal{L}(W_1^t; (logits, y))$   $\triangleright$  Update visual feature weights by cross-entropy loss  $\mathcal{L}(\cdot)$  and SGD
19: end for
```

---